THE JOURNAL OF PHYSICAL CHEMISTRY A

Article

pubs.acs.org/JPCA

Mesospheric Removal of Very Long-Lived Greenhouse Gases SF_6 and CFC-115 by Metal Reactions, Lyman-α Photolysis, and Electron Attachment

Anna Totterdill,[†] Tamás Kovács,[†] Juan Carlos Gómez Martín,[†] Wuhu Feng,[†,‡] and John M. C. Plane*[,†]

[†]School of Chemistry, University of Leeds, Leeds LS2 9JT, U.K.

[‡]National Centre for Atmospheric Science, School of Earth and Environment, University of Leeds, Leeds LS2 9JT, U.K.

ABSTRACT: The fluorinated gases SF_6 and C_2F_5Cl (CFC-115) are chemically inert with atmospheric lifetimes of many centuries which, combined with their strong absorption of IR radiation, results in unusually high global warming potentials. Very long lifetimes imply that mesospheric sinks could make important contributions to their atmospheric removal. In order to investigate this, the photolysis cross sections at the prominent solar Lyman-α emission line (121.6 nm), and the reaction kinetics of SF_6 and CFC-115 with the neutral meteoric metal atoms Na, K, Mg, and Fe over large temperature ranges, were measured experimentally. The Na and K reactions exhibit significant non-Arrhenius behavior; quantum chemistry calculations of the potential energy surfaces for the SF_6 reactions indicate that the Na and K reactions with SF_6 are probably activated by vibrational excitation of the F-SF_5 (ν_3) stretching mode. A limited set of kinetic measurements on Na + SF_5CF_3 are also presented. The atmospheric removal of these long-lived gases by a variety of processes is then evaluated. For SF_6, the removal processes in decreasing order of importance are electron attachment, VUV photolysis, and reaction with K, Na, and H. For CFC-115, the removal processes in decreasing order of importance are reaction with $O(^1D)$, VUV photolysis, and reaction with Na, K, and H.

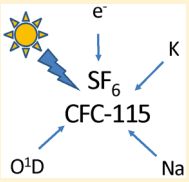

1. INTRODUCTION

Characterizing the atmospheric lifetimes (τ) of the perfluorinated compounds (PFCs), SF_6, SF_5CF_3, and C_2F_5Cl (CFC-115), is a crucial step in assessing their potential impact on global warming. These PFCs are potent greenhouse gases which possess large global warming potentials (GWPs) resulting from a combination of strong infrared absorptions in the atmospheric window and very long atmospheric lifetimes. Species for which $\tau \geq 300$ years may be predominantly destroyed in the mesosphere by processes such as far-UV photolysis[1] and electron attachment,[2] requiring general circulation models to account for their transport into the upper stratosphere and mesosphere.[3]

To date, the most potent greenhouse gas to have been reviewed by the Intergovernmental Panel on Climate Change (IPCC) is SF_6, which has a projected lifetime of 3200 years with a 100 year GWP of 23500.[4,5] Industrial applications of SF_6 are primarily in fluid insulation, electronics, and switchgears.[6] Its long lifetime together with increasing industrial usage has led to a marked increase in the atmospheric mixing ratio of SF_6. The gas was not detected in the atmosphere prior to its usage in industry, indicating it to be entirely anthropogenic. Its current tropospheric mixing ratio is around 8 ppt, increasing at an average rate of 0.26 ppt yr^{-1} since 1995.[7]

SF_5CF_3 is a very potent greenhouse gas, with a long atmospheric lifetime of approximately 800 years and a GWP in the region of 17500.[8] Although not used industrially, this gas appears to be a byproduct of the manufacture of fluorosurfactants. CFC-115 was initially introduced as a refrigerant in the 1970s and prior to this was not detected in the atmosphere. Maione et al.[9] reported a 2011 concentration of 8.4 ppt; following its proscription, a decreasing trend of 0.01 ppt y^{-1} has been observed.[9] CFC-115 has a currently estimated 100 year GWP of 7370 based on the atmospheric lifetime used by the IPCC of 1020 years.[5] However, this lifetime has since been revised to 540 years following the re-evaluation of its removal by reaction with $O(^1D)$.[10]

In this paper, we consider mesospheric removal processes of these PFCs which could potentially lead to an overestimate of atmospheric lifetimes if ignored. We first address the potential reactions between the PFCs and the metal atoms which are injected into the upper mesosphere by cosmic dust ablation.[11] The most abundant of these metals are Fe, Na, Mg, and K, which occur in layers between 80 and 105 km with peak concentrations of approximately 10000, 5000, 3000, and 80 cm^{-3}, respectively.[12] In order to quantify the potential role of metal atoms in the atmospheric lifetimes of these PFCs, in this study we report rate constant measurements of the following reactions:

$$Na + SF_6 \rightarrow NaF + SF_5 \quad \Delta H_r(298\ K) = -85\ kJ\ mol^{-1} \tag{R1}$$

$$Na + SF_5CF_3 \rightarrow NaF + SF_4CF_3 \quad \Delta H_r(298\ K) = -102\ kJ\ mol^{-1} \tag{R2}$$

Received: December 11, 2014
Revised: February 3, 2015
Published: February 3, 2015

DOI: 10.1021/jp5123344
J. Phys. Chem. A 2015, 119, 2016−2025

$$Na + CF_3CF_2Cl \rightarrow NaCl + CF_3CF_2$$
$$\Delta H_r(298\ K) = -131\ kJ\ mol^{-1} \quad (R3)$$

$$K + SF_6 \rightarrow KF + SF_5 \quad \Delta H_r(298\ K) = -97\ kJ\ mol^{-1} \quad (R4)$$

$$K + CF_3CF_2Cl \rightarrow KCl + CF_3CF_2$$
$$\Delta H_r(298\ K) = -143\ kJ\ mol^{-1} \quad (R5)$$

$$Fe + SF_6 \rightarrow FeF + SF_5 \quad \Delta H_r(298\ K) = -55\ kJ\ mol^{-1} \quad (R6)$$

$$Mg + SF_6 \rightarrow MgF + SF_5 \quad \Delta H_r(298\ K) = -71\ kJ\ mol^{-1} \quad (R7)$$

The significant exothermicities of these reactions are calculated from a compilation of bond energies,[13] except for the enthalpy change for reaction R2 which was calculated using electronic structure theory (see Discussion). Calculations at the same level of theory show that the formation of SF_5CF_2 in reaction R2 is endothermic by 17 kJ mol^{-1}, so that this reaction channel should not be important over the temperature range in this study. The choice of the four metals is therefore based on their mesospheric abundance and the fact that these reactions are all exothermic.

Apart from reactions R1 and R4 which have been studied previously (though with apparently significant disagreement in the case of the Na + SF_6 reaction),[14−16] the kinetics of the other reactions do not appear to have been measured. We then discuss the complex temperature dependencies of the Na and K reactions in some detail. In addition, we report measurements of the Lyman-α (121.6 nm) absorption cross sections of SF_6 and CFC-115. Photolysis is currently recognized as the major sink of SF_6,[1] though with a significant contribution from electron attachment in the upper mesosphere and lower thermosphere.[3] Photolysis and electron attachment are also considered to be the major loss routes for SF_5CF_3.[17] Note that due to a limited supply of SF_5CF_3, we only report a study of reaction R2 for this PFC.

In order to assess the impacts of our new results on the atmospheric lifetimes of SF_6 and CFC-115, the loss rates of the metal atom reactions and VUV photolysis are then compared with the loss rates due to associative and dissociative attachment of electrons to SF_6[18,19] and the reaction of $O(^1D)$ atoms with CFC-115.[20] Note that the vertical electron affinity of CFC-115 is −1.3 eV (calculated using the level of theory described in Discussion), so that thermal electron attachment to this PFC is not significant. The rate constant for the reaction of $O(^1D)$ with SF_6 has an upper limit of 1.8×10^{-14} cm^3 $molecule^{-1}$ s^{-1},[21] which is consistent with an endothermicity of 38 kJ mol^{-1}.[13] These two processes are therefore not considered further.

2. EXPERIMENTAL SECTION

A detailed description of the experimental techniques used for the metal atom kinetic studies, including the choice of photolytic precursors, is provided in our earlier paper on the reactions of Na, K, Mg, and Fe with NF_3.[22] Reaction R1 was studied at 290 K using a stainless steel fast flow tube (FFT). An aluminum oxide crucible housed within a tungsten basket heater containing pure sodium chips was located within the flow tube, downstream of the carrier gas inlet, and was heated to approximately 500 K. The resulting Na vapor was then entrained in the flow of N_2 carrier gas and carried downstream where it mixed with varying ratios of SF_6 in N_2. The relative Na concentration was measured by laser-induced fluorescence (LIF) at 589 nm. Reactions R1−R7 were studied over the range of 201−875 K, using the pulsed laser photolysis-laser-induced fluorescence (PLP-LIF) technique. Rate constants were obtained by measuring the LIF decay rates of metal atoms generated by excimer laser photolysis of a metal-containing precursor in the presence of varying concentrations of reactant gas.

The Lyman-α (121.6 nm) absorption cross sections of SF_6 and CFC-115 were measured using an absorption cell coupled to a H_2/He radiofrequency discharge light source, as described elsewhere.[22]

Materials. Reactant gas mixtures for the experiments were prepared on all-glass vacuum lines. The gases N_2 (99.9999%, BOC), SF_6 (99.99%, BOC), and He (99.9999%, BOC) were used without further purification. Samples of CFC-115 and SF_5CF_3 were provided by Professor William Sturges (University of East Anglia). These were purified by freeze−thaw-distillation on a glass vacuum line and the purity confirmed by IR spectroscopy. The metal-atom precursors, sodium (98% Sigma-Aldrich), sodium iodide (Sigma-Aldrich 98%), potassium iodide (Sigma-Aldrich 99%), magnesium acetyl acetonate (Sigma-Aldrich 98%), and ferrocene (Sigma-Aldrich 98%), were purified under vacuum (heating where appropriate) for at least an hour before kinetic experiments commenced, as described previously.[22]

3. RESULTS

3.1. Metal Atom Reactions. In the FFT study of reaction R1, SF_6 was kept in excess of Na, ensuring pseudo first-order conditions, resulting in the following expression:

$$k't = -\ln\left(\frac{[Na]^t_{SF_6}}{[Na]^t_0}\right) = -\ln\left(\frac{S^t_{SF_6}}{S^t_0}\right) \quad (E1)$$

where k' is the pseudo first order loss rate, t is the contact time, and $[Na]_{SF_6}{}^t$ and $[Na]^t_0$ are the Na concentrations with and without SF_6 present at time t, respectively. $S_{SF_6}{}^t$ and S^t_0 are the LIF signals proportional to these concentrations. The contact time, t is calculated from the plug flow velocity calculated from the mass flow rate and pressure, reduced by 5% to account for gas mixing by diffusion and with the centroid correction coefficient (0.63) applied to correct for the parabolic flow profile within the tube.[22,23] We have shown previously,[24] using the pulsed ablation of metal targets in the same flow tube, that these corrections produce an accurate estimate (within 4%) of the contact time. Six measurements of $k't$ were taken at different contact times, from which a rate constant of $k_1(290\ K) = (9.83 \pm 0.61) \times 10^{-13}$ cm^3 $molecule^{-1}$ s^{-1} was obtained.

In the PLP-LIF experiments, the PFC (SF_6 or CFC-115) was also maintained in excess over the metal atoms to ensure pseudo first-order conditions. This resulted in the LIF signal decaying exponentially with time:

$$\frac{[X]_t}{[X]_0} = \frac{S_t}{S_0} = \exp(-k't) \quad (E2)$$

where $[X]_t$ and $[X]_0$ are the concentrations of metal atom X (X = Na, K, Mg, or Fe), with corresponding LIF signals S_t and S_0, at the delays t and 0, respectively.

DOI: 10.1021/jp5123344
J. Phys. Chem. A 2015, 119, 2016−2025

The loss rate of metal is described by the pseudo first-order decay coefficient k':

$$k' = k'_{diff} + k[PFC] \quad \text{(E3)}$$

where k'_{diff} represents the diffusion of metal atoms out of the dye laser beam volume within the field of view of the photomultiplier tube and k is the second-order rate constant.

From E3, a plot of k' against [PFC] yields a line with slope k and intercept k'_{diff}. Figure 1 shows bimolecular plots for R1 at

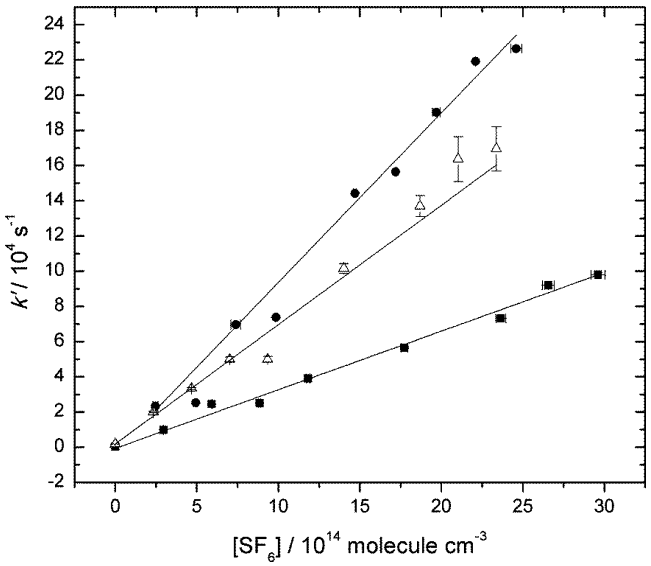

Figure 1. Bimolecular plots used to determine the rate constants for the reaction between Na and SF_6 at 585 K (■), 717 K (△), and 879 K (●), measured by the PLP-LIF technique.

three temperatures (585, 717, and 879 K). Second-order rate constants for R1−R7 were measured over the range of temperatures listed in Tables 1, 2, 3, 4, 5, 6, and 7, respectively,

Table 1. Rate Constants for R1 (Na + SF_6)

T (K)	k (10^{-12} cm^3 molecule^{-1} s^{-1})
212	(0.10 ± 0.01)
248	(0.40 ± 0.04)
290	(0.98 ± 0.06)[a]
327	(1.86 ± 0.15)
396	(4.63 ± 0.44)
418	(4.53 ± 0.34)
429	(6.31 ± 0.29)
539	(15.81 ± 1.27)
585	(32.76 ± 1.30)
637	(59.72 ± 8.18)
717	(68.52 ± 5.67)
771	(32.76 ± 1.30)
879	(87.89 ± 0.49)

[a]Rate constants measured with the fast flow tube. All other measurements were made using the PLP-LIF technique.

where the given uncertainty encompasses the error of the weighted least-squares linear fits to the kinetic plots and the uncertainty in the concentration of gas mixtures.

3.2. Lyman-α Absorption. Examples of the absorbance data for SF_6 and CFC-115 as a function of concentration are shown in Figure 2. Linear regression analysis yielded $\sigma(SF_6, 121.6\ nm) = (1.37 \pm 0.12) \times 10^{-18}$ cm^2 and σ(CFC-115, 121.6 nm) = $(4.27 \pm 0.35) \times 10^{-18}$ cm^2, where the uncertainties are at the 95% confidence level and include the uncertainty in gas concentration.

Table 2. Rate Constants for R2 (Na + SF_5CF_3)

T (K)	k (10^{-12} cm^3 molecule^{-1} s^{-1})
327	(2.50 ± 0.07)
373	(4.40 ± 0.32)
417	(7.84 ± 0.86)
588	(30.08 ± 1.29)
630	(51.56 ± 8.31)
714	(67.93 ± 5.12)
875	(94.16 ± 4.97)

Table 3. Rate Constants for R3 (Na + CF_3CF_2Cl)

T (K)	k (10^{-13} cm^3 molecule^{-1} s^{-1})
248	(0.04 ± 0.01)
342	(0.41 ± 0.07)
416	(1.18 ± 0.11)
477	(2.88 ± 0.26)
573	(9.29 ± 0.82)
685	(22.77 ± 2.14)
868	(50.92 ± 6.90)

Table 4. Rate Constants for R4 (K + SF_6)

T (K)	k (10^{-11} cm^3 molecule^{-1} s^{-1})
207	(1.21 ± 0.11)
248	(2.07 ± 0.22)
320	(3.16 ± 0.28)
340	(3.49 ± 0.32)
388	(7.13 ± 0.62)
450	(9.16 ± 0.78)
486	(10.96 ± 0.94)
522	(11.73 ± 0.10)
566	(15.49 ± 1.43)
687	(25.39 ± 2.15)
817	(28.39 ± 2.57)

Table 5. Rate Constants for R5 (K + CF_3CF_2Cl)

T (K)	k (10^{-12} cm^3 molecule^{-1} s^{-1})
350	(0.81 ± 0.16)
372	(1.00 ± 0.20)
423	(1.65 ± 0.34)
468	(3.15 ± 0.34)
515	(4.15 ± 0.71)
586	(7.08 ± 1.24)
710	(18.23 ± 2.74)
851	(19.60 ± 2.21)

Table 6. Rate Constants for R6 (Fe + SF_6)

T (K)	k (10^{-15} cm^3 molecule^{-1} s^{-1})
350	(0.92 ± 0.30)
396	(2.18 ± 0.33)
429	(3.53 ± 0.38)
461	(4.06 ± 0.73)
486	(7.40 ± 1.12)
583	(21.31 ± 4.35)

DOI: 10.1021/jp5123344
J. Phys. Chem. A 2015, 119, 2016−2025

Table 7. Rate Constants for R7 (Mg + SF_6)

T (K)	k (10^{-14} cm^3 molecule^{-1} s^{-1})
449	(0.23 ± 0.09)
568	(1.11 ± 0.39)
631	(2.54 ± 0.65)
738	(9.38 ± 1.52)
792	(23.60 ± 4.26)

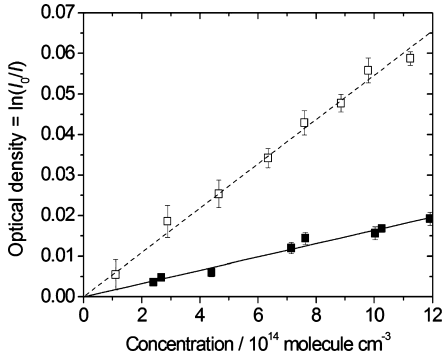

Figure 2. Beer–Lambert plots for the measured optical densities of SF_6 (filled symbols and solid line fit) and CFC-115 (open symbols and dashed line fit). The path length was 12.4 cm.

4. DISCUSSION

4.1. Reactions with Metal Atoms. Arrhenius plots describing the temperature dependence of the rate constants for R1–R7 are illustrated in Figures 3–5. Reactions R1, R3, and

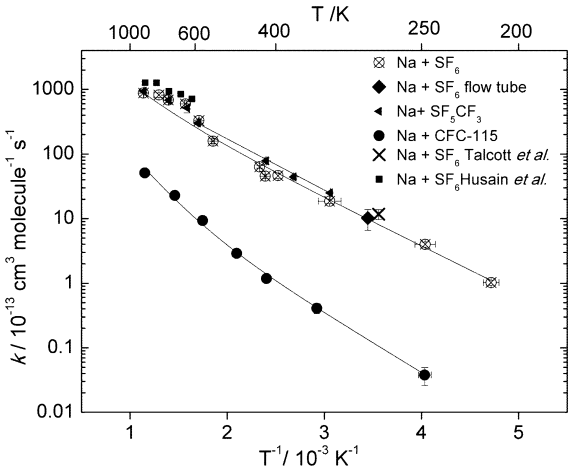

Figure 3. Arrhenius plots for the reactions of Na with SF_6, SF_5CF_3, and CFC-115. All measurements were made using the PLP-LIF technique, apart from the single flow tube measurement in the present study and previous measurements of k(Na + SF_6) by Talcott et al.[14] and Husain and et al.[16] (see the figure legend).

R4 exhibit non-Arrhenius behavior, so their rate constants were expressed as the sum of two Arrhenius terms which capture the high- and low-temperature regimes:

$$k(T) = A\exp(-B/RT) + C\exp(-D/RT) \quad \text{(E4)}$$

where A and C represent the pre-exponential terms of the high and low temperature regimes, respectively, and B and D are the respective activation energies (R is the gas constant):

$$k_1(\mathrm{Na} + \mathrm{SF_6},\ 212 - 879\ \mathrm{K}) = (19.0 \pm 17.2) \times 10^{-10} \exp[-(28.7 \pm 6.7)\ \mathrm{kJ\ mol^{-1}}/RT] + (3.58 \pm 0.08) \times 10^{-10} \exp[-(14.3 \pm 0.5)\ \mathrm{kJ\ mol^{-1}}/RT]\ \mathrm{cm^3\ molecule^{-1}\ s^{-1}}$$

$$k_3(\mathrm{Na} + \mathrm{C_2F_5Cl},\ 248 - 868\ \mathrm{K}) = (5.92 \pm 3.45) \times 10^{-10} \exp[-(35.4 \pm 3.2)\ \mathrm{kJ\ mol^{-1}}/RT] + (1.84 \pm 0.14) \times 10^{-11} \exp[-(17.4 \pm 0.3)\ \mathrm{kJ\ mol^{-1}}/RT]\ \mathrm{cm^3\ molecule^{-1}\ s^{-1}}$$

$$k_4(\mathrm{K} + \mathrm{SF_6},\ 207 - 817\ \mathrm{K}) = (27.7 \pm 9.6) \times 10^{-10} \exp[-(16.8 \pm 1.7)\ \mathrm{kJ\ mol^{-1}}/RT] + (1.79 \pm 0.20) \times 10^{-10} \exp[-(4.44 \pm 0.25)\ \mathrm{kJ\ mol^{-1}}/RT]\ \mathrm{cm^3\ molecule^{-1}\ s^{-1}}$$

These expressions were obtained by first fitting a subset of low-temperature rate constants to a single Arrhenius term (i.e., determining parameters C and D), and then fitting the complete data set to E4 to obtain A and B. The extent of the low-temperature regime was determined by performing an iterative calculation where data points were incorporated stepwise to the low temperature subset to ensure a physically sensible value for A (set to an upper limit of 3×10^{-9} cm^3 molecule^{-1} s^{-1}). Approximately 75% and 60% of the uncertainty in the high-temperature pre-exponential factor and activation energy terms, respectively, are attributable to the full data set fit, with the remainder propagating from the low temperature fit.

No significant curvature was observed in the other reactions, and these were fitted to single Arrhenius term expressions:

$$k_2(\mathrm{Na} + \mathrm{SF_5CF_3},\ 327 - 875\ \mathrm{K}) = (6.61 \pm 0.78) \times 10^{-10} \exp[-(15.2 \pm 0.4)\ \mathrm{kJ\ mol^{-1}}/RT]\ \mathrm{cm^3\ molecule^{-1}\ s^{-1}}$$

$$k_5(\mathrm{K} + \mathrm{C_2F_5Cl},\ 350 - 851\ \mathrm{K}) = (1.86 \pm 0.40) \times 10^{-10} \exp[-(16.0 \pm 0.8)\ \mathrm{kJ\ mol^{-1}}/RT]\ \mathrm{cm^3\ molecule^{-1}\ s^{-1}}$$

$$k_6(\mathrm{Fe} + \mathrm{SF_6},\ 350 - 583\ \mathrm{K}) = (1.90 \pm 1.01) \times 10^{-12} \exp[-(22.5 \pm 1.9)\ \mathrm{kJ\ mol^{-1}}/RT]\ \mathrm{cm^3\ molecule^{-1}\ s^{-1}}$$

$$k_7(\mathrm{Mg} + \mathrm{SF_6},\ 449 - 792\ \mathrm{K}) = (1.15 \pm 1.10) \times 10^{-10} \exp[-(42.6 \pm 5.5)\ \mathrm{kJ\ mol^{-1}}/RT]\ \mathrm{cm^3\ molecule^{-1}\ s^{-1}}$$

These fits to the experimental data points are shown in Figures 3–5. Inspection of Figures 3 and 4 show that Na and K react significantly faster with SF_6 than C_2F_5Cl, and the K reactions are ~5–120 times faster than the corresponding Na reactions at the same temperature. The rate constants for Na + SF_6 and Na + SF_5CF_3 are almost identical (Figure 3). Figure 5 shows

DOI: 10.1021/jp5123344
J. Phys. Chem. A 2015, 119, 2016–2025

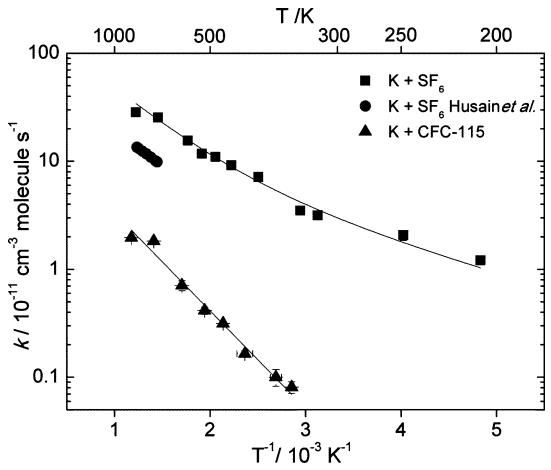

Figure 4. Arrhenius plots for the reactions of K with SF_6 and CFC-115. A previous measurement of k(K + SF_6) by Husain and Lee[15] is also shown.

that Mg and Fe are comparatively unreactive compared to the Group 1 metal atoms.

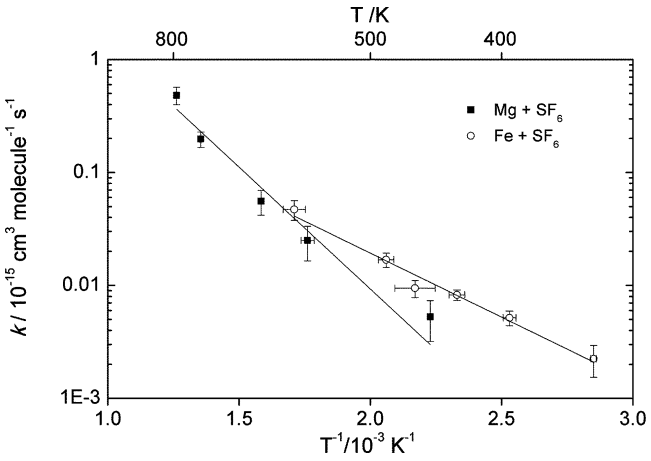

Figure 5. Arrhenius plots for the reactions of Fe and Mg with SF_6.

In the present study of R1 (Na + SF_6), the results obtained with the FFT and PLP-LIF techniques at 290 K are consistent (Table 1). R1 has been studied previously by Talcott et al.[14] in a flow tube study at 281 K and by Husain and Marshall[16] in a flash photolysis/resonance absorption study over the temperature range 644−918 K. Figure 3 shows that our results are in very good agreement with both previous studies. R1 has also been studied in a diffusion flame, from which a rate constant of k_1(523 K) = 3.6×10^{-11} cm^3 molecule^{-1} s^{-1} was obtained (see Table 1 in Gislason and Kwei[25]), which is a factor of 2.3 larger than in the present study. Düren et al.[26] measured a reaction cross section σ = 46 Å^2 at a collision velocity $v = 3.1 \times 10^5$ cm s^{-1} (which corresponds to a kinetic temperature of 8670 K). Expressing the rate constant as the product $\sigma \times v$ yields an estimate of k(8670 K) ∼ 1.4×10^{-9} cm^3 molecule^{-1} s^{-1}, which is in surprisingly good agreement with an extrapolated value of 1.6×10^{-9} cm^3 molecule^{-1} s^{-1} using the Arrhenius fit above.

The reaction kinetics of R4 (K + SF_6) have been studied previously by Husain et al.[15] over the temperature range of 691−810 K. Figure 4 shows that although the activation energy at high temperature is similar to that from the present study, the rate constants are approximately 2.3 times smaller. The reason for this significant difference is unclear, particularly given the good agreement for R1 between the two techniques. The reaction cross section for R4 has also been measured in two molecular beam studies. Airey et al.[27] measured σ = 60 Å^2 at a collision velocity $v = 6.8 \times 10^4$ cm s^{-1}, equivalent to k_4(677 K) ∼ 4.1×10^{-10} cm^3 molecule^{-1} s^{-1}, which is a factor of 1.9 times larger than measured in the present study. Sloane et al.[28] obtained σ = 55 Å^2 at a collision velocity $v = 6.9 \times 10^4$ cm s^{-1}, equivalent to k_4(687 K) ∼ 3.8×10^{-10} cm^3 molecule^{-1} s^{-1}, which is a factor of 1.7 times larger than the present measurements. The agreement is therefore quite satisfactory. Sloane et al.[28] showed in their beam-gas experiment that the reaction cross section increased by a factor of 1.5 when the SF_6 temperature was increased from 300 to 580 K, from which they concluded that excitation of the stretching modes of SF_6 enhanced its reactivity toward K. Additionally, Riley and Herschbach[29] showed that the differential cross sections exhibit roughly symmetrical forward and backward scattering, indicating that the reaction proceeds via a collision complex which persists for at least several rotational periods.

Although reactions R1−R7 are quite exothermic (see Introduction), their rate constants are in general significantly smaller than their respective collision frequencies at 300 K [e.g., k(K + SF_6) is a factor of ∼10 smaller], k(Na + SF_6) is smaller by ∼2 orders of magnitude, and the other reactions are even slower. In order to gain deeper insight into the metal atom + SF_6 kinetics, potential energy surfaces (PESs) for the Na, K, and Mg + SF_6 reactions were calculated at the MP2(full)/6-311+g(2d) level of theory using the Gaussian 09 suite of programs.[30] At this level of theory, the calculated reaction enthalpy changes (including a counterpoise correction for basis set superposition error) agree very well with the literature values[13] shown in parentheses: $\Delta_r H^{\ominus}$(Na + SF_6) = −90 (−85); $\Delta_r H^{\ominus}$(K + SF_6) = −98 (−97); and $\Delta_r H^{\ominus}$(Mg + SF_6) = −74 (−71) kJ mol^{-1}. The Møller−Plesset correlation energy correction and this choice of basis set therefore seems to provide reasonably accurate energies over these surfaces where there is a switch from the covalent character in the entrance channel to ionic character in the exit channel where the metal fluoride forms. At each point on the PES, a new initial guess for the Hartree−Fock wave function was generated to ensure that the lowest energy surface was chosen. <S^2> values ranged from 0.750 to 0.763 on the Na and K + SF_6 surfaces, demonstrating little spin contamination in the unrestricted Hartree−Fock calculations used for these surfaces.

Figure 6 shows PESs for the three reactions (not including zero-point energies). These surfaces illustrate the case where the metal atom attack is collinear with one of the S−F bonds. The scan is therefore along the S−F−M (M = metal atom) linear coordinate, where r_{S-F} and r_{M-F} are varied. Since the geometry of the SF_5 moiety is frozen in these scans, the surface does not represent the lowest possible energy path from reactants to products. However, the difference is not significant: for the Mg + SF_6 surface, the fully optimized transition state has a barrier of 48 kJ mol^{-1}, which is only 3 kJ mol^{-1} lower than the barrier shown in Figure 6c. This is because the SF_5 geometry does not change significantly between SF_5−F and SF_5 + F; the energy of the frozen SF_5 geometry is only 12 kJ mol^{-1} above that of the optimized geometry.

The three PESs exhibit late barriers in their exit channels, particularly Mg + SF_6 (Figure 6c). The barriers increase in the order of K (16 kJ mol^{-1}), Na (24 kJ mol^{-1}), and Mg (51 kJ

DOI: 10.1021/jp5123344
J. Phys. Chem. A 2015, 119, 2016−2025

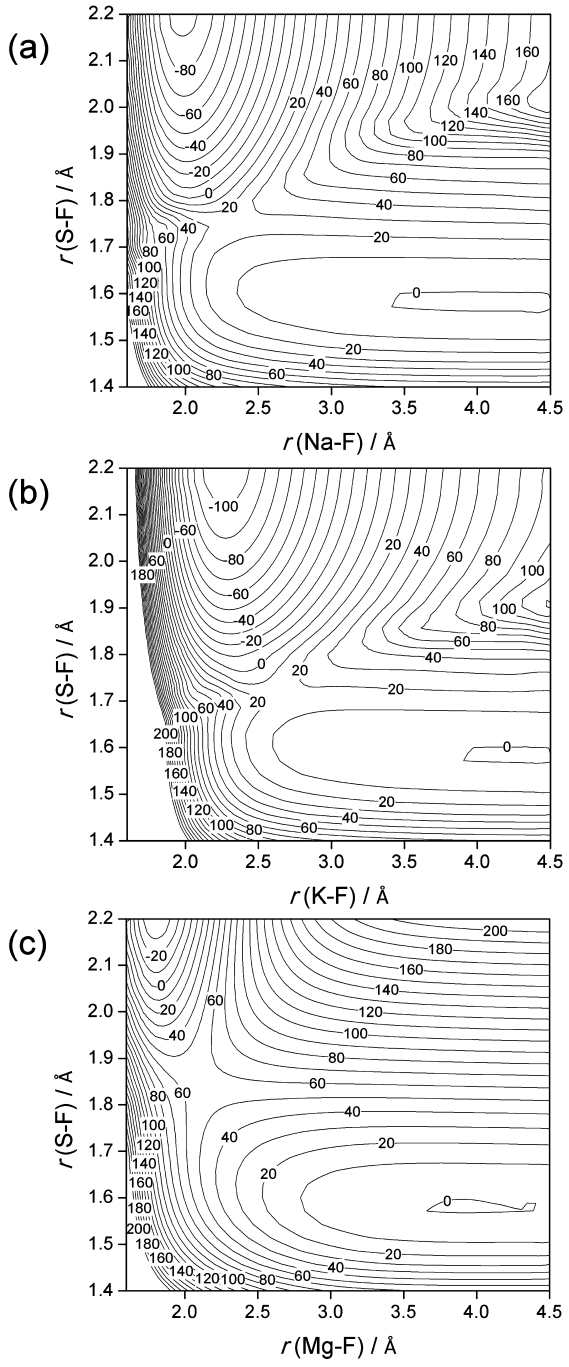

Figure 6. Potential energy surfaces for Na, K, and Mg + SF_6 calculated at the MP2(FULL)/6-311+g(2d,p) level of theory. These surfaces are for the case where the metal atom attack is collinear with one of the S−F bonds. The scan is therefore along the S−F−M(etal atom) linear coordinate, where r(S−F) and r(M−F) are varied. Note that the geometry of the SF_5 moiety is frozen, which means that the surface does not represent the lowest possible energy path from reactants to products.

mol^{-1}), which is the same order in which the rate constants decrease (Figures 3−5). The optimized energy barrier for Mg + SF_6, including zero-point energy is 39 kJ mol^{-1} (or 43 kJ mol^{-1} including the thermal energy at 298 K). These values are in good accord with the experimental activation energy of 42.6 ± 5.5 kJ mol^{-1} (see above). For K and Na, the barrier heights including ZPE are 13 and 19 kJ mol^{-1}, respectively. These energies lie in between the two activation energies obtained from the biexponential Arrhenius fits for these reactions.

Reactions with late barriers tend to be activated by vibrational excitation in a reactant bond corresponding to the reaction coordinate.[31] Acknowledging that the detailed non-Arrhenius behavior of R1, R3, and R4 is obscured by the scatter of the data and that there is a risk of overinterpretation of the biexponential fitted parameters, it is still tempting to link the difference in activation energies between the low and temperature regimes to the role of vibrational excitation in activating these reactions. The Arrhenius expressions for k_1 and k_4 (see above) exhibit an increase in activation energy between the low and high temperature terms of (14.4 ± 7.2) and (12.4 ± 2.0) kJ mol^{-1}, respectively. These differences correspond (within error) to one quantum of the asymmetric ν_3 S−F stretching mode of SF_6 at 940 cm^{-1},[32] which is equivalent to 11.2 kJ mol^{-1}. This is consistent with the first term in each Arrhenius expression containing the probability of ν_3 excitation: for example, the Boltzmann population of SF_6 (ν_3 > 0) increases from only 3.3% at 300 K to 37.5% at 700 K. As mentioned earlier, the role of SF_6 vibration in enhancing the reaction cross section for reaction R4 (K + SF_6) was proposed to explain the molecular beam results of Sloane et al.[28] Similarly, the activation energy increase of k_3 is (15.0 ± 7.2) kJ mol^{-1}. This corresponds within error to one quantum of the 982 cm^{-1} (11.7 kJ mol^{-1}) asymmetric stretching mode[33] of CFC-115, which most closely resembles the reaction coordinate. It is noteworthy that non-Arrhenius behavior was also observed in our previous study of Na and K reacting with NF_3.[22]

4.2. VUV Photolysis. The Lyman-α absorption cross section of SF_6 from the present study is $\sigma(SF_6, 121.6\ nm) = (1.37 \pm 0.12) \times 10^{-18}$ cm^2. Previous measurements in chronological order are 2.74×10^{-18} cm^2 by Bastien et al.,[34] $(1.76 \pm 0.13) \times 10^{-18}$ cm^2 by Ravishankara et al.,[1] 1.83×10^{-18} cm^2 by Pradayrol et al.,[35] and 1.20×10^{-18} cm^2 by Zetzch.[36] The earliest measurement by Bastien et al. appears to be an outlier; however, it is not clear why the four most recent measurements vary by about 50%. Our value is reasonably close to the average of 1.5×10^{-18} cm^2.

The absorption cross section for CFC-115 from the present study is σ(CFC-115, 121.6 nm) = $(4.27 \pm 0.35) \times 10^{-18}$ cm^2. This is significantly smaller than a very old measurement of 1.76×10^{-17} cm^2 by Doucet et al.[37] but in excellent agreement with a value of $(4.57 \pm 0.37) \times 10^{-18}$ cm^2 measured by Ravishankara et al.[1] In order to assess the role of photolysis in the atmosphere, the absorption cross sections over the VUV spectral range are required. Previous measurements of the SF_6 cross sections over the 116−180 nm and 121−125 nm ranges were reported by Pradayrol et al.[35] and Zetzsch,[36] respectively. For CFC-115, the only reported measurements between 122 and 172 nm are by Doucet et al.[37] As noted above, their measurement at 121.6 nm is about a factor of 4 times larger than the present study. In contrast, at 172 nm Doucet et al.[37] are in good agreement with the recent JPL recommendation[21] (which extends to 230 nm). Since the cross section between 122 and 170 nm (i.e., not including Lyman-α) does not make a significant contribution to the photodissociation rate of CFC-115 (see Figure 7), we have therefore used the Doucet et al.[37] results over this range without scaling them downward to match the Lyman-α measurements from the present study and that of Ravishankara et al.[1]

DOI: 10.1021/jp5123344
J. Phys. Chem. A 2015, 119, 2016−2025

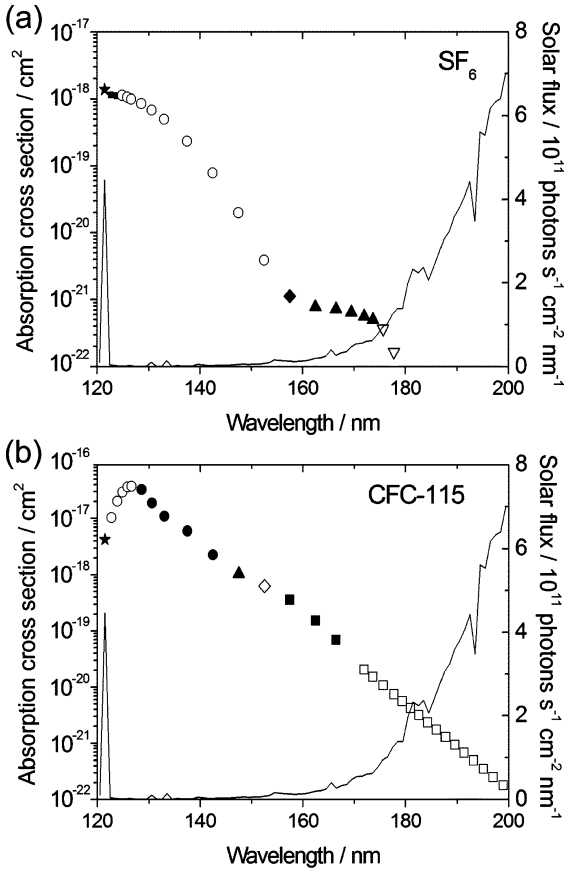

Figure 7. (a) SF_6 absorption cross sections (left-hand ordinate): present study (121.6 nm, ★); fit to Zetzch et al.[36] (115−125 nm, ■); fits to Pradayrol et al.[35] (125−155 nm, ○; 155−160 nm, ◆; 160−175 nm, ▲; 175−180 nm, △, see text for further details). The solid line is the solar spectral irradiance (right-hand ordinate). (b) CFC-115 absorption cross section (left-hand ordinate): present study (121.6 nm, filled star); fits to Doucet et al.[37] (121.6−127 nm, ○; 127−142 nm, ●; 146−172 nm, ▲, ◇, and ■); JPL recommendation[21] (172−230 nm, □). The solid line is the solar spectral irradiance (right-hand ordinate).

We have derived the following polynomial expressions describing the cross section as a function of wavelength from composite data sets containing our cross section at 121.6 nm and the literature values (see above) at longer UV wavelengths. For SF_6: σ(115−125 nm) = $\exp(1.061 \times 10^{-2}\lambda^2 - 2.644\lambda + 123.4)$; σ(125−155 nm) = $\exp(-5.420 \times 10^{-3}\lambda^2 + 1.298\lambda - 118.9)$; σ(155−160 nm) = $\exp(1.458 \times 10^{-2}\lambda^2 - 4.762\lambda + 340.1)$; σ(160−175 nm) = $\exp(-2.870 \times 10^{-3}\lambda^2 + 0.9264\lambda - 123.3)$; σ(175−180 nm) = $\exp(-3.425 \times 10^{-2}\lambda^2 + 11.73\lambda - 1053)$ cm^2. For CFC-115: σ(121.6−128 nm) = $\exp(-9.141 \times 10^{-2}\lambda^2 + 23.13\lambda - 1.501 \times 10^3)$; σ(128−132 nm) = $\exp(3.221 \times 10^{-2}\lambda^2 - 8.631\lambda + 539.3)$; σ(132−144 nm) = $\exp(-6.301 \times 10^{-3}\lambda^2 + 1.570\lambda - 136.4)$; σ(144−150 nm) = $\exp(-0.1274\lambda - 22.61)$; σ(150−154 nm) = $\exp(-2.880 \times 10^{-2}\lambda - 37.51)$; σ(154−172 nm) = $\exp(-3.061 \times 10^{-3}\lambda^2 + 0.8080\lambda - 93.80)$; σ(172−230 nm)/cm^2 = $2.521 \times 10^{-7} \exp(-\lambda/5.705)$

Figure 7 shows the resulting cross sections as a function of wavelength, together with the solar irradiance, which emphasizes the importance of the Lyman-α line in the solar spectrum.

5. ATMOSPHERIC IMPLICATIONS

In addition to photolysis and the reactions with metal atoms which have been investigated in this study, a number of other processes remove SF_6 and CFC-115. These are electron attachment to SF_6, which is considered in more detail below, and the reaction between CFC-115 and O(^{1}D):

$$C_2F_5Cl + O(^1D) \rightarrow ClO + C_2F_5 \quad \text{(R8)}$$

Reaction R8 is fast with an overall (i.e., quenching + reaction) rate constant of $k(217-373\ \text{K}) = 6.5 \times 10^{-11} \exp(+30/T)$ cm^3 molecule^{-1} s^{-1} and a reactive yield of 0.72.[20] This reaction, as shown below, is important in the stratosphere where photolysis of O_3 leads to relatively high concentrations of O(^{1}D). In the middle and upper mesosphere there are significant concentrations of O(^{3}P) and H,[38] so we have calculated the reaction enthalpies and transition state energies for the following reactions using the accurate CBS-QB3 level of theory:[39]

$$C_2F_5Cl + O(^3P) \rightarrow ClO + C_2F_5 \quad \Delta H_r^{\ominus}(298\text{K}) = +103\ \text{kJ mol}^{-1} \quad \text{(R9)}$$

$$C_2F_5Cl + H \rightarrow HCl + C_2F_5 \quad \Delta H_r^{\ominus}(298\text{K}) = -67\ \text{kJ mol}^{-1} \quad \text{(R10)}$$

$$SF_6 + O(^3P,^1D) \rightarrow FO + C_2F_5 \quad \Delta H_r^{\ominus}(298\ \text{K}) = +228\ \text{kJ mol}^{-1}, 38\ \text{kJ mol}^{-1} \quad \text{(R11)}$$

$$SF_6 + H \rightarrow HF + C_2F_5 \quad \Delta H_r^{\ominus}(298\ \text{K}) = -125\ \text{kJ mol}^{-1} \quad \text{(R12)}$$

Note that although reactions R10 and R12 are exothermic, they both have significant calculated transition state energies (including zero-point energies) of 44 and 103 kJ mol^{-1}, respectively, and so will not be important at atmospheric temperatures. Reaction R11 is too endothermic even for the reaction of SF_6 with O(^{1}D), which is 190 kJ mol^{-1} above the ground state, to be possible, in contrast to the reaction of C_2F_5Cl with O(^{1}D).

5.1. Thermal Electron Attachment to SF_6. Low-energy electrons are in thermal equilibrium with the surrounding gas in the upper mesosphere and lower thermosphere.[38] Below 80 km, electrons are mostly attached to molecules in the form of negative ions, such as HCO_3^- and NO_3^-. Because the electron detachment energies from these ions are larger than the electron affinity of SF_6, only direct attachment of free electrons will lead to the potential destruction of SF_6 via two pathways: associative attachment to form the SF_6^- anion, which can then either undergo photodetachment or react with various compounds; and dissociative attachment to form SF_5^- + F.[40]

Both associative and dissociative electron attachment have been treated in detail in a series of recent papers by Troe and co-workers.[18,19] The net associative attachment rate coefficient, k_{at}, at an atmospheric density [N_2 + O_2] and temperature T is given by the following expression[18] which neglects radiative stabilization (since this is only important at much lower pressures) and assumes that O_2 has a similar efficiency to N_2:

$$k_{at} = \frac{x}{1+x} F_c^{\left[1+\log_{10}\left(\frac{x}{N}\right)^2\right]^{-1}} \quad \text{(E5)}$$

where x is the ratio of the low- to the high-pressure limiting rate coefficients (i.e., $x = k_{at,0}/k_{at,\infty}$), where

DOI: 10.1021/jp5123344
J. Phys. Chem. A 2015, 119, 2016−2025

$$k_{at,0} = [N_2 + O_2]2.5 \times 10^{-18} \exp(-T/80\ \mathrm{K}) \times [1 + 3.5 \times 10^{-22}(T/\mathrm{K})^7]\ \mathrm{cm^3\ molecule^{-1}\ s^{-1}} \quad \text{(E6)}$$

and

$$k_{at,\infty} = 2.20 \times 10^{-7}(T/500\ \mathrm{K})^{-0.35}\ \mathrm{cm^3\ molecule^{-1}\ s^{-1}} \quad \text{(E7)}$$

The temperature dependence of the broadening factor F_c is given by

$$F_c = \exp(-T/520\ \mathrm{K}) \quad \text{(E8)}$$

and the parameter N is given by

$$N = 0.75 - 1.27 \log_{10}(F_c) \quad \text{(E9)}$$

Chemical removal of SF_6^- can either recycle or remove SF_6.[3] The removal reactions are

$$SF_6^- + H \rightarrow \text{products} \qquad k_9 = 2.1 \times 10^{-10}\ \mathrm{cm^3\ molecule^{-1}\ s^{-1}}\ \text{(ref 3)} \quad \text{(R13)}$$

$$SF_6^- + HCl \rightarrow \text{products} \qquad k_{10} = 1.5 \times 10^{-9}\ \mathrm{cm^3\ molecule^{-1}\ s^{-1}}\ \text{(ref 40)} \quad \text{(R14)}$$

while the recycling channels are

$$SF_6^- + O_3 \rightarrow SF_6 + O_3^- \qquad k_{11} = 1.2 \times 10^{-9}\ \mathrm{cm^3\ s^{-1}}\ \text{(ref 40)} \quad \text{(R15)}$$

$$SF_6^- + O \rightarrow SF_6 + O^- \qquad k_{12} = 1.4 \times 10^{-10}\ \mathrm{cm^3\ s^{-1}}\ \text{(ref 40)} \quad \text{(R16)}$$

The photodetachment coefficient for SF_6^- (J_{PD}) can be estimated by integrating the product of the electron photodetachment cross section and the extra-terrestrial solar irradiance from 280 to 700 nm,[41] assuming a quantum yield of unity. The cross section was calculated by combining the recent theoretical spectrum of Eisfeld[42] with absolute experimental values reported by Bopp et al.,[43] Christophorou and Olthoff,[44] and Datskos et al.[45] This gives a midday value of 1.1 s^{-1} at 85 km.

Assuming that SF_6^- is in steady state, the permanent removal rate of SF_6 by associative electron attachment becomes $k_{EA}[SF_6][e^-]$, where

$$k_{EA} = k_{at}\frac{k_{13}[H] + k_{14}[HCl]}{J_{PD} + k_{13}[H] + k_{14}[HCl] + k_{15}[O_3] + k_{16}[O]} \quad \text{(E10)}$$

Second we consider the dissociative channel. At pressures above 10^{-4} Torr, the branching ratio $\beta(P,T)$ for the dissociative thermal electron attachment channel for SF_6 is very small (~0.001).[3,46,47] Troe et al.[19] (in their Figure 9) show that at a pressure of 10^{-2} Torr (corresponding to an altitude of ~80 km), the fraction that dissociates is less than 10^{-4}. The dissociative electron attachment removal rate as a function of temperature can be obtained by fitting an Arrhenius expression to the 10^{-2} Torr line in this figure, over the temperature range of 200–320 K where an Arrhenius plot is reasonably linear. This results in the following expression:

$$\beta(10^{-2}\ \mathrm{Torr}, T) = e^{(-4587/T+7.74)} \quad \text{(E11)}$$

The pressure-dependent results at 300 K from Troe et al.[19] can then be combined with the data point from Foster and Beauchamp[48] at 1.5×10^{-7} Torr to yield a pressure-dependent expression for β at 300 K:

$$\log_{10}[\beta(P, 300\ \mathrm{K})] = -4.362 - 0.582 \log_{10}(P/\mathrm{Torr}) - 0.0203[\log_{10}(P/\mathrm{Torr})]^2 \quad \text{(E12)}$$

Troe et al.[19] have shown that the pressure dependence of β is very similar over a range of temperatures between 200 and 300 K. Therefore, eq E12 can be used to scale eq E11 by normalizing to $\beta(10^{-2}\ \mathrm{Torr}, 300\ \mathrm{K}) = 5.26 \times 10^{-4}$, producing an expression for β as a function of both T and P:

$$\beta(P, T) = e^{\{-4587/T+7.74)} \times 10^{(4.362-0.582\log_{10}(P/\mathrm{torr})-0.0203[\log_{10}(P/\mathrm{torr})]^2/5.26\times10^{-4}\}} \quad \text{(E13)}$$

Finally,

$$\beta(P, T) = \frac{k_{dis}}{k_{dis} + k_{at}} \quad \text{(E14)}$$

so that k_{dis} can be calculated from k_{at} (eq E5).

Figure 8 illustrates the variation of β with altitude and also shows the atmospheric temperature profile (a global average for January 2010, see below). β is at a minimum around the tropopause, where the relatively low temperature and high pressure causes associative attachment to dominate. In contrast, at the high temperatures and low pressures of the lower thermosphere (above 115 km), dissociative attachment dominates and β approaches unity. In the mesosphere between 50 and 100 km, β is approximately constant because the effect of decreasing temperature is offset by the decreasing pressure.

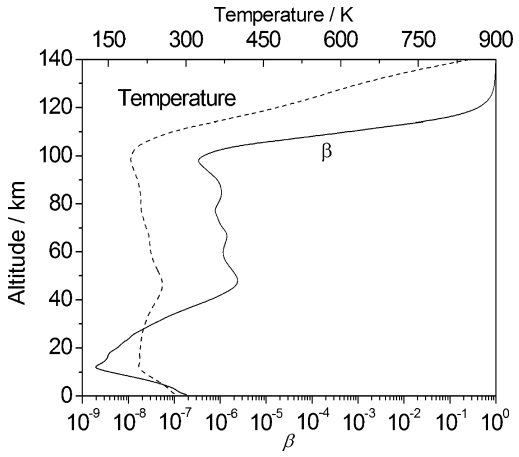

Figure 8. SF_5^-/SF_6^- branching ratio for thermal electron attachment to SF_6. The vertical profiles of atmospheric density and temperature are global averages obtained from the WACCM model (see text).

The loss rates of SF_6 and CFC-115 as a function of altitude, due to the various processes discussed above, are illustrated in Figure 9. The photolysis rates of SF_6 and CFC-115 were calculated using the scheme described in our earlier study on NF_3.[22] The Na and K profiles are taken from recent implementations of Na and K chemistry in the Whole Atmosphere Community Climate Model (WACCM).[49,50]

DOI: 10.1021/jp5123344
J. Phys. Chem. A 2015, 119, 2016–2025

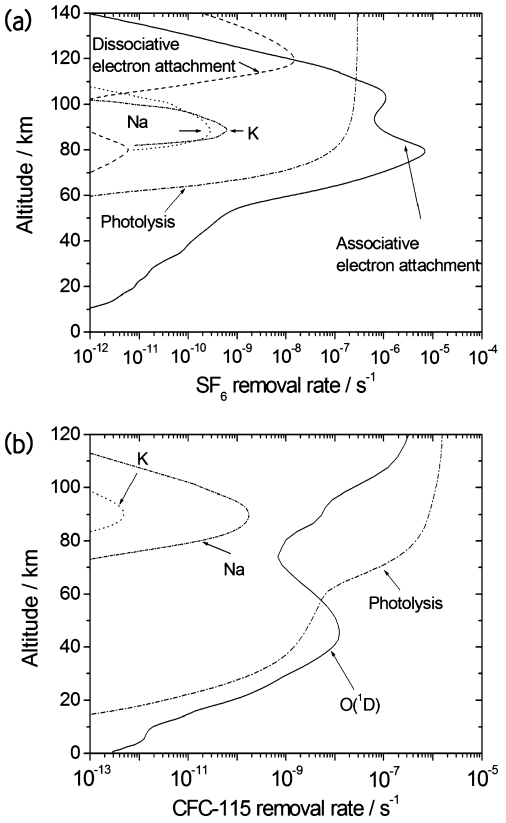

Figure 9. (a) First-order removal rates of CFC-115 by photolysis (dash−dot line) and reaction with $O(^1D)$ (solid line), Na (short dash−dot line) and K (dotted line). (b) First-order removal rates of SF_6 by photolysis (dash−dot line), associative electron attachment (solid line), dissociative electron attachment (dashed line); reaction with Na (short dash−dot line) and reaction with K (dotted line).

This chemistry-climate model was also used to provide vertical profiles of the H, HCl, O_3, H, $O(^1D)$, and electron density. For illustrative purposes, we have taken the global averages of these parameters for January, 2010. Figure 9 demonstrates that the Na and K reactions are not competitive in the removal of either SF_6 or CFC-115. Figure 9a shows that associative electron attachment is the dominant removal process for SF_6 throughout the atmosphere up to 110 km; at higher altitudes, photolysis dominates. Nevertheless, the absolute loss rate by electron attachment only becomes significant in the mesosphere where the removal rate exceeds 10^{-9} s^{-1} (*e*-folding lifetime < 30 years). Combining this slow rate of removal with the time taken to transport SF_6 above 50 km[3] explains the exceptionally long atmospheric lifetime of SF_6 (see Introduction). In the case of CFC-115, Figure 9b shows that reaction with $O(^1D)$ is the major removal process, up to 50 km. This process peaks in the upper stratosphere around 40 km; this is where there is a maximum in $O(^1D)$ because the O_3 concentration on the topside of the O_3 layer is still high enough for relatively rapid photochemical production of $O(^1D)$, but the total atmospheric density is low enough that electronic quenching of $O(^1D)$ is comparatively slow.[38] Thus, the lifetime of CFC-115 is considerably shorter than that of SF_6.

6. CONCLUSIONS

This study has explored the impact of a number of processes which can remove the long-lived greenhouse gases SF_6 and CFC-115 in the mesosphere. Despite the reactions of Na, K, Fe, and Mg with these PFCs being significantly exothermic, the reactions have substantial barriers on their respective potential energies which cause the reactions to be too slow at the temperatures of the upper mesosphere (<230 K) to contribute significantly to the removal of the PFCs. Theoretical calculations indicate that the Na and K reactions with SF_6 may be activated by vibrational excitation of the F-SF_6 (ν_3) asymmetric stretching mode. A limited set of measurements on Na + SF_5CF_3 indicates that this PFC behaves very much like SF_6.

The Lyman-α absorption cross sections for SF_6 and CFC-115 were also measured and found to be in generally good agreement with the more recent previous studies.[1,35,36] Although VUV photolysis of SF_6 is the major loss process above 105 km, below this height associative electron attachment dominates and so this is the process which controls the atmospheric lifetime of this PFC. In the case of CFC-115, VUV photolysis is the major loss process above 60 km, but the removal of this species by reaction with $O(^1D)$ dominates in the stratosphere and hence controls its lifetime.

AUTHOR INFORMATION

Corresponding Author

*E-mail: J.M.C.Plane@leeds.ac.uk.

Notes

The authors declare no competing financial interest.

ACKNOWLEDGMENTS

This work was part of the MAPLE project (PI: Professor Martyn Chipperfield) funded by research Grant NE/J008621/1 from the U.K. Natural Environment Research Council, which also provided a studentship for A.T. We thank Prof. William Sturges (University of East Anglia) for supplying samples of CFC-115 and SF_5CF_3.

REFERENCES

(1) Ravishankara, A. R.; Solomon, S.; Turnipseed, A. A.; Warren, R. F. Atmospheric Lifetimes of Long-Lived Halogenated Species. *Science* **1993**, *259*, 194−199.

(2) Morris, R. A.; Viggiano, A. A.; Arnold, S. T.; Paulson, J. F. Chemistry of Atmospheric Ions Reacting with Fully Fluorinated Compounds. *Int. J. Mass Spectrom. Ion Processes* **1995**, *149−150*, 287−298.

(3) Reddmann, T.; Ruhnke, R.; Kouker, W. Three-Dimensonal Model Simulations of SF_6 with Mesospheric Chemistry. *J. Geophys. Res.* **2001**, *106*, 14,525−14,537.

(4) IPCC. *Climate Change 2013: The Physical Science Basis. Contribution of Working Group I to the Fifth Assessment Report of the Intergovernmental Panel on Climate Change*; Cambridge University Press: Cambridge, United Kingdom, 2013.

(5) Solomon, S.; Qin, D.; Manning, M.; Chen, Z.; Marquis, M.; Averyt, K.B.; Tignor, M.; Miller, H. L. *Contribution of Working Group I to the Fourth Assessment Report of the Intergovernmental Panel on Climate Change*; Cambridge University Press: Cambridge, 2007; Vol. *IV*.

(6) Preisegger, E.; Durschner, R.; Klotz, W.; Konig, C. A.; Krahling, H.; Neumann, C.; Zahn, B. *Life Cycle Assessment - Electricity Supply Using SF_6 Technology*; Springer: Dordrecht, The Netherlands, 2000.

(7) Stiller, G. P.; von Clarmann, T.; Hoepfner, M.; Glatthor, N.; Grabowski, U.; Kellmann, S.; Kleinert, A.; Linden, A.; Milz, M.; Reddmann, T.; et al. Global Distribution of Mean Age of Stratospheric Air from MIPAS SF_6 Measurements. *Atmos. Chem. Phys.* **2008**, *8*, 677−695.

DOI: 10.1021/jp5123344
J. Phys. Chem. A 2015, 119, 2016−2025

(8) Tsai, W.-T. The Prediction of Environmental Fate for Trifluoromethyl Sulfur Pentafluoride (SF_5CF_3), a Potent Greenhouse Gas. *J. Haz. Mater.* **2007**, *149*, 747−751.
(9) Maione, M.; Giostra, U.; Arduini, J.; Furlani, F.; Graziosi, F.; Lo Vullo, E.; Bonasoni, P. Ten Years of Continuous Observations of Stratospheric Ozone Depleting Gases at Monte Cimone (Italy): Comments on the Effectiveness of the Montreal Protocol from a Regional Perspective. *Sci. Total Environ.* **2013**, *445*, 155−164.
(10) Lifetimes of Stratospheric Ozone-Depleting Substances, Their Replacements, and Related Species; Ko, M. K. W., Newman, P. A., Reimann, S., Strahan, S. E., Eds.; *SPARC Report No. 6*, WCRP-15/2013, 2013.
(11) Vondrak, T.; Plane, J. M. C.; Broadley, S.; Janches, D. A Chemical Model of Meteoric Ablation. *Atmos. Chem. Phys.* **2008**, *8*, 7015−7032.
(12) Plane, J. M. C. Atmospheric Chemistry of Meteoric Metals. *Chem. Rev.* **2003**, *103*, 4963−4984.
(13) Lide, D. R. *Handbook of Physics and Chemistry*; CRC Press: Boca Raton, FL, 2006; Vol. *87*.
(14) Talcott, C. L.; Ager, J. W.; Howard, C. J. Gas Phase Studies of Na Diffusion in He and Ar and Kinetics of Na + CI_2 and Na + SF_6. *J. Chem. Phys.* **1986**, *84*, 6161−6169.
(15) Husain, D.; Lee, Y. H. Measurement of Absolute Rate Data for the Reaction of Atomic Potassium, $K(4^2S_{1/2})$, with CF_3Cl, CF_2Cl_2, $CFCl_3$, CF_3Br and SF_6 as a Function of Temperature by Time-Resolved Atomic Resonance Absorption Spectroscopy at [λ] = 404 nm [$K(5^2P_J)$ - $K(4^2S_{1/2})$]. *J. Chem. Soc., Faraday Trans. 2* **1987**, *83*, 2325−2337.
(16) Husain, D.; Marshall, P. Determination of Absolute Rate Data for the Reaction of Atomic Sodium, $Na(3^2S_{1/2})$, with CF_3Cl, CF_2Cl_2, $CFCl_3$, CF_3Br and SF_6 as a Function of Temperature by Time-resolved Atomic Resonance Absorption Spectroscopy at 589nm [$Na(3^2P_J) \rightarrow Na(3^2S_{1/2})$]. *J. Chem. Soc., Faraday Trans.* **1985**, *81*, 613−624.
(17) Takahashi, K.; Nakayama, T.; Matsumi, Y.; Solomon, S.; Gejo, T.; Shigemasa, E.; Wallington, T. J. Atmospheric lifetime of SF_5CF_3. *Geophys. Res. Lett.* **2002**, *29*, No. 1712.
(18) Troe, J.; Miller, T. M.; Viggiano, A. A. Low-Energy Electron Attachment to SF_6. I. Kinetic Modeling of Non-Dissociative Attachment. *J. Chem. Phys.* **2007**, *127*, No. 244303.
(19) Troe, J.; Miller, T. M.; Viggiano, A. A. Low-Energy Electron Attachment to SF_6. II. Temperature and Pressure Dependences of Dissociative Attachment. *J. Chem. Phys.* **2007**, *127*, No. 244304.
(20) Baasandorj, M.; Fleming, E. L.; Jackman, C. H.; Burkholder, J. B. $O(^1D)$ Kinetic Study of Key Ozone Depleting Substances and Greenhouse Gases. *J. Phys. Chem. A* **2013**, *117*, 2434−2445.
(21) Sander, S. P.; Abbatt, J.; Barker, J. R.; Burkholder, J. B.; Friedl, R. R.; Golden, D. M.; Huie, R. E.; Kolb, C. E.; Kurylo, M. J.; Moortgat, G. K. et al. *Chemical Kinetics and Photochemical Data for Use in Atmospheric Studies*; Evaluation No. 17, JPL Publication 10-6, Jet Propulsion Laboratory: Pasadena, CA, 2011.
(22) Totterdill, A.; Gómez Martín, J. C.; Kovács, T.; Feng, W.; Plane, J. M. C. Experimental Study of the Mesospheric Removal of NF_3 by Neutral Meteoric Metals and Lyman-α Radiation. *J. Phys. Chem. A* **2014**, 4120−4129.
(23) Howard, C. J. Kinetic Measurements Using Flow Tubes. *J. Phys. Chem.* **1978**, *83*, 3−9.
(24) Self, D. E.; Plane, J. M. C. A Kinetic Study of the Reactions of Iron Oxides and Hydroxides Relevant to the Chemistry of Iron in the Upper Mesosphere. *Phys. Chem. Chem. Phys.* **2003**, *5*, 1407−1418.
(25) Gislason, E. A.; Kwei, G. H. Quenching of Glory Undulations in Scattering of Na Atoms from Polyhalide Molecules. *J. Chem. Phys.* **1967**, *46*, 2838−2840.
(26) Düren, R.; Färber, M.; Heumann, B.; Knepper, M.; Mohr, S.; Weiss, C.; Te Lintel Hekkert, S.; Linskens, A. F.; Reuss, J. Differential Cross Sections for State Specific Reactive Scattering of Na + $SF_6 \rightarrow$ NaF+ SF_5. *J. Chem. Phys.* **1996**, *104*, 3620−3628.
(27) Airey, J. R.; Greene, E. F.; Reck, G. P.; Ross, J. Scattering of Potassium by a Series of Reactive and Nonreactive Compounds in Crossed Molecular Beams. *J. Chem. Phys.* **1967**, *46*, 3295−3305.
(28) Sloane, T. M.; Tang, S. Y.; Ross, J. Dependence of Reactivity on Internal and Translational Energy in K + SF_6, CCl_4, and $SnCl_4$. *J. Chem. Phys.* **1972**, *57*, 2745−2755.
(29) Riley, S. J.; Herschbach, D. R. Molecular Beam Kinetics: Long-Lived Collision Complexes in Reactions of K, Rb, and Cs with $SnCl_4$ and SF_6. *J. Chem. Phys.* **1973**, *58*, 27−43.
(30) Frisch, M. J.; Trucks, G. W.; Schlegel, H. B.; Scuseria, G. E.; Robb, M. A.; Cheeseman, J. R.; Scalmani, G.; Barone, V.; Mennucci, B.; Petersson, G. A. et al. *Gaussian 09*, revision A.1; Gaussian, Inc.: Wallingford CT, 2009.
(31) Smith, I. W. M. *Kinetics and Dynamics of Elementary Gas Reactions*; Butterworths: London, 1980.
(32) Lagemann, R. T.; Jones, E. A. The Infrared Spectrum of Sulfur Hexafluoride. *J. Chem. Phys.* **1951**, *19*, 534−536.
(33) Nielson, J. R.; Liang, C. Y.; Smith, R. M. Infrared and Raman Spectra of Fluorinated Ethanes. 5. The series CF_3CF_3, CF_3CF_2Cl, CF_3CFCl_2, and CF_3CCl_3. *J. Chem. Phys.* **1953**, *21*, 383−393.
(34) Bastien, F.; Chatterton, P. A.; Marode, E.; Moruzzi, J. L. Photoabsorption Measurements in SF_6, SF_6 Mixtures and Some Fluorocarbon Gases. *J. Phys. D* **1985**, *18*, 1327−1337.
(35) Pradayrol, C.; Casanovas, A. M.; Deharo, I.; Guelfucci, J. P.; Casanovas, J. Absorption Coefficients of SF_6, SF_4, SOF_2 and SO_2F_2 in the Vacuum Ultraviolet. *J. Phys. III* **1996**, *6*, 603−612.
(36) Zetzsch, C. *UV Absorption Cross Sections of Sulfur Hexafluoride and Acetonitrile*; DEEPAK Publishing: Hampton, 1989.
(37) Doucet, J.; Sauvegeau, P.; Sandorfy, C. Photoelectron and Far-Ultraviolet Absorption Spectra of Chlorofluoro Derivatives of Ethane. *J. Chem. Phys.* **1975**, *62*, 335−359.
(38) Brasseur, G. P.; Solomon, S. *Aeronomy of the Middle Atmosphere*; Springer: New York, 2005.
(39) Montgomery, J. A.; Frisch, M. J.; Ochterski, J. W.; Petersson, G. A. A Complete Basis Set Model Chemistry. VI. Use of Density Functional Geometries and Frequencies. *J. Chem. Phys.* **1999**, *110*, 2822−2827.
(40) Huey, L. G.; Hanson, D. R.; Howard, C. J. Reactions of SF_6^- and I^- with Atmospheric Trace Gases. *J. Phys. Chem.* **1995**, *99*, 5001−5008.
(41) Gueymard, C. A. The Sun's Total and Spectral Irradiance for Solar Energy Applications and Solar Radiation Models. *Sol. Energy* **2004**, *76*, 423−453.
(42) Eisfeld, W. Highly Accurate Determination of the Electron Affinity of SF_6 and Analysis of Structure and Photodetachment Spectrum of SF_6. *J. Chem. Phys.* **2011**, *134*, No. 054303.
(43) Bopp, J. C.; Roscioli, J. R.; Johnson, M. A.; Miller, T. M.; Viggiano, A. A.; Villano, S. M.; Wren, S. W.; Lineberger, W. C. Spectroscopic Characterization of the Isolated SF_6^- and $C_4F_8^-$ Anions: Observation of Very Long Harmonic Progressions in Symmetric Deformation Modes upon Photodetachment. *J. Phys. Chem. A* **2007**, *111*, 1214−1221.
(44) Christophorou, L. G.; Olthoff, J. K. Electron Interactions with SF_6. *J. Phys. Chem. Ref. Data* **2000**, *29*, 267−330.
(45) Datskos, P. G.; Carter, J. G.; Christophorou, L. G. Photodetachment of SF_6^-. *Chem. Phys. Lett.* **1995**, *239*, 38−43.
(46) Fehsenfeld, F. C. Electron Attachment to SF_6. *J. Chem. Phys.* **1970**, *53*, 2000−2004.
(47) Miller, T. M.; Miller, A. E. S.; Paulson, J. F.; Liu, X. Thermal Electron Attachment to SF_4 and SF_6. *J. Chem. Phys.* **1994**, *100*, 8841−8848.
(48) Foster, M. S.; Beauchamp, J. Electron Attachment to Sulphur Hexafluoride: Formation of Stable SF_6 at Low Pressure. *Chem. Phys. Lett.* **1975**, *31*, 482−485.
(49) Marsh, D. R.; Janches, D.; Feng, W.; Plane, J. M. C. A Global Model of Meteoric Sodium. *J. Geophys. Res.* **2013**, *118*, 11,442−11,452.
(50) Plane, J. M. C.; Feng, W.; Dawkins, E.; Chipperfield, M. P.; Höffner, J.; Janches, D.; Marsh, D. R. Resolving the Strange Behavior of Extraterrestrial Potassium in the Upper Atmosphere. *Geophys. Res. Lett.* **2014**, *41*, 4753−4760.

DOI: 10.1021/jp5123344
J. Phys. Chem. A 2015, 119, 2016−2025